DOI: 10.15669/pnst.8.262

Progress in Nuclear Science and Technology
Volume 8 (2025) pp. 262-267

ARTICLE

Evaluation of Dissolution Behavior of Platinum Group Alloys in the Presence of Liquid Waste

Sayaka CHIBA [1], Haruaki MATSUURA [1*], Isamu SATO [1],
Haruka TADA [2] and Hiroki IZUMI [2]

[1] *Tokyo City University, 1-28-1 Tamazutsumi, Setagaya-ku, Tokyo, 158-8557, Japan*
[2] *IHI Corporation, TOYOSU IHI BUILDING, 1-1, Toyosu 3-chome, Koto-ku, Tokyo, 135-8710, Japan*

In order to evaluate the dissolution behavior of platinum group alloys (Mo-Ru-Rh-Pd-Tc) remaining in undissolved residue liquid waste in spent fuel reprocessing, simulated liquid waste or 2.0 M nitric acid and simulated platinum group alloy samples were used. Various compositions of alloy samples were dissolved at room temperature. It was confirmed that the alloy was dissolved to a depth from the surface on the order of nanometers, and it was found that part of the Mo reacted with the liquid waste component, but the rest of the elements remained in the metallic state at depths from the surface of over 2 nm.

KEYWORDS: undissolved residue, platinum group alloy, liquid waste, dissolution behavior, Mo, Ru, Rh, Pd, EXAFS, XPS

I. Introduction

In spent fuel reprocessing, platinum group alloys (Mo-Ru-Rh-Pd-Tc) are contained in the undissolved residue of liquid waste.[1,2)] The undissolved residue liquid waste is stored for a long time in a solution along with high-level concentrated liquid waste and alkaline liquid waste, and then fed into a glass melter. The platinum group alloys in the glass melter settle and accumulate at the bottom of the melter since their solubility is low in the molten glass.[3)] As a result, electrical resistance in the glass drops,[4)] and the temperature inside the melter decreases. In addition, the decrease in the flowability of the glass and the blockage of the melter nozzle due to the formation of yellow phase are also affected by the platinum group alloys.[5)] Therefore, it is important to understand the behavior of platinum group alloys during the vitrification process, and we focused on these alloys in this study.

In the future, it is predicted that the composition of platinum group alloys will fluctuate with variation in fuel burnup. Accordingly, the dissolution behavior of platinum group alloys in the liquid waste may also change. Furthermore, after the dissolution step, in the process where the undissolved residue is mixed with other liquid wastes and stored, the composition and structure of the platinum group alloys may further change due to dissolution. Previous work has confirmed that the oxidation behavior of platinum group alloys coexisting with glass and liquid waste and the transition to glass depend on the alloy composition,[6)] and the alloy composition is one of the important parameters. Therefore, as part of the study of the effect of fluctuations in spent fuel on the vitrification process, it is necessary to investigate the dissolution behavior of platinum group alloys due to compositional fluctuation.

In addition, Matsui[7)] showed that as the ratio of Ru increased, the overall solubility rate also decreased. However, since his study assumed a dissolving tank, the conditions were set for high temperatures, high concentrations, and short periods. Also, liquid waste was not taken into account for evaluation of dissolution behavior.

Therefore, in this study, we conducted two platinum group alloy dissolution tests to elucidate the dissolution behavior of platinum group alloys coexisting with liquid waste, and we analyzed the concentration of the dissolved solution to understand three points: the amount of dissolution; the structural changes before and after dissolution as reflected in the crystal structure and local structure analysis of the residue; and the structural changes before and after dissolution, focusing on the surface as reflected in the surface analysis of the residue. In the first test, a powder alloy sample was used to simulate the platinum group alloys present in the liquid waste with a particle size of several tens of nanometers to several micrometers. In addition, we expected that the effect of dissolution would increase as the surface area increased. On the other hand, in the second test, a plate-shaped alloy sample was used. This second test was intended to take into account two points: that there was a variation in the particle size of the powdered sample which influenced the effect appearing; and that surface analysis was difficult with the powder.

II. Experimental

1. Dissolution Test of Alloy Powder Samples

Regarding the various alloy composition samples, R5-2 simulated MOX and high burnup spent fuel, R5-4 simulated the fuel in widest use before burning, and R5-5 simulated fuel with an increased Mo ratio for comparison. In addition, we determined a simulated composition of spent fuel using the ORNL Isotope Generation and Depletion Code, Origen2 (version 2.1).[7,8)] The compositions (wt%) of three specific simulated alloy samples were: R5-2 (Mo, 15; Ru, 55; Rh, 15; Pd, 15); R5-4 (Mo, 20; Ru, 60; Rh, 10; Pd, 10); and R5-5 (Mo, 30; Ru, 50; Rh, 10; Pd 10). Mo, Ru, Rh, and Pd metal powders (purity 99.9%; Niraco Co., Ltd.) were weighed out according to the above compositions, mixed well, and pressed, before being alloyed by arc melting. Arc melting was performed three times for 30 s at a current of about 50 A. An automatic stamping mill (ADA-48, Ito Manufacturing Co., Ltd.) and a planetary ball mill (P-6, Fritsch) were used to process the powder into a finer powder with a particle size of several tens of micrometers or less. **Figure 1** shows an image of the fine-powdered R5-2 obtained using a scanning electron microscope (SEM) (TM3000, Hitachi High-Technologies Co., Ltd.). From Fig. 1, we confirmed that the fine-powdered alloy had particles of ~30 μm.

*Corresponding author, E-mail: g2381810@tcu.a

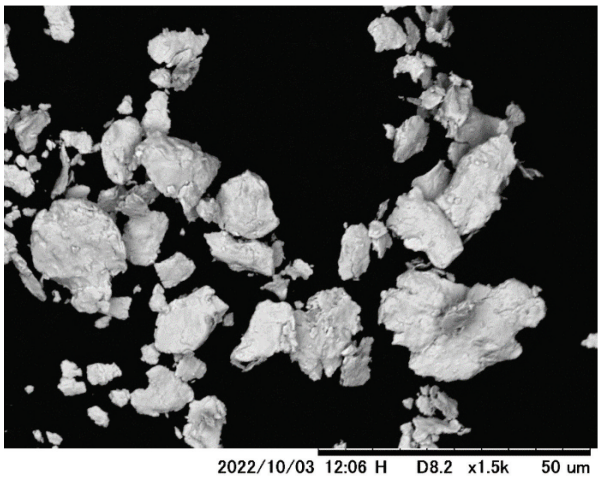

Fig. 1 x1500 SEM image of R5-2 sample

A magnetic stirring bar and 0.3 g of the powdered simulated alloy were placed in a beaker. Thereafter, 50 ml of 2.0 M nitric acid or liquid waste simulant (**Table 1**) was added, and a dissolution test of powder was conducted for 10 days or 100 days while using the magnetic stirring bar. The temperature was room temperature (about 25°C) during the powder dissolution test.

After the powder dissolution test was completed, the solution and the residue were separated by gravity using a separation filter and filter paper. The concentration of each alloy component was analyzed for the dissolved solution using inductively coupled plasma optical emission spectrometry (ICP-OES) (CIROS-120, Rigaku Co.) and ICP mass spectrometry (ICP-MS) (MS7700x, Agilent Technologies). In addition, the dried residue was subjected to crystal structure analysis using x-ray diffraction (XRD) (M03XHF², Bruker AXS). An X-ray absorption fine structure (XAFS) instrument (BL27B, High Energy Accelerator Research Organization) was used to analyze the locstructure

Table 1 Composition of liquid waste simulant

Element	Concentration [mol/L]	Oxide equivalent [g/L]	Element	Concentration [mol/L]	Oxide equivalent [g/L]
H	2.00E+00	-	Na	7.94E-01	24.62
Ag	1.29E-03	0.15	Nd	1.15E-01	19.36
Ba	2.71E-02	4.15	Ni	4.32E-02	3.23
Ce	3.41E-02	5.87	P	2.54E-03	0.18
Co	1.43E-02	1.07	Pr	1.66E-02	2.83
Cr	7.89E-04	0.06	Rb	8.99E-03	0.84
Cs	3.75E-02	5.29	Sb	2.74E-04	0.04
Eu	1.70E-03	0.30	Sm	1.07E-02	1.86
Fe	8.92E-02	7.12	Sn	1.46E-03	0.22
Gd	5.44E-02	9.86	Sr	1.92E-02	1.99
La	1.85E-02	3.01	Te	7.64E-03	1.22
Mn	3.48E-02	2.47	Y	1.12E-02	1.27
Mo	7.29E-02	10.49	Zr	8.51E-02	10.48

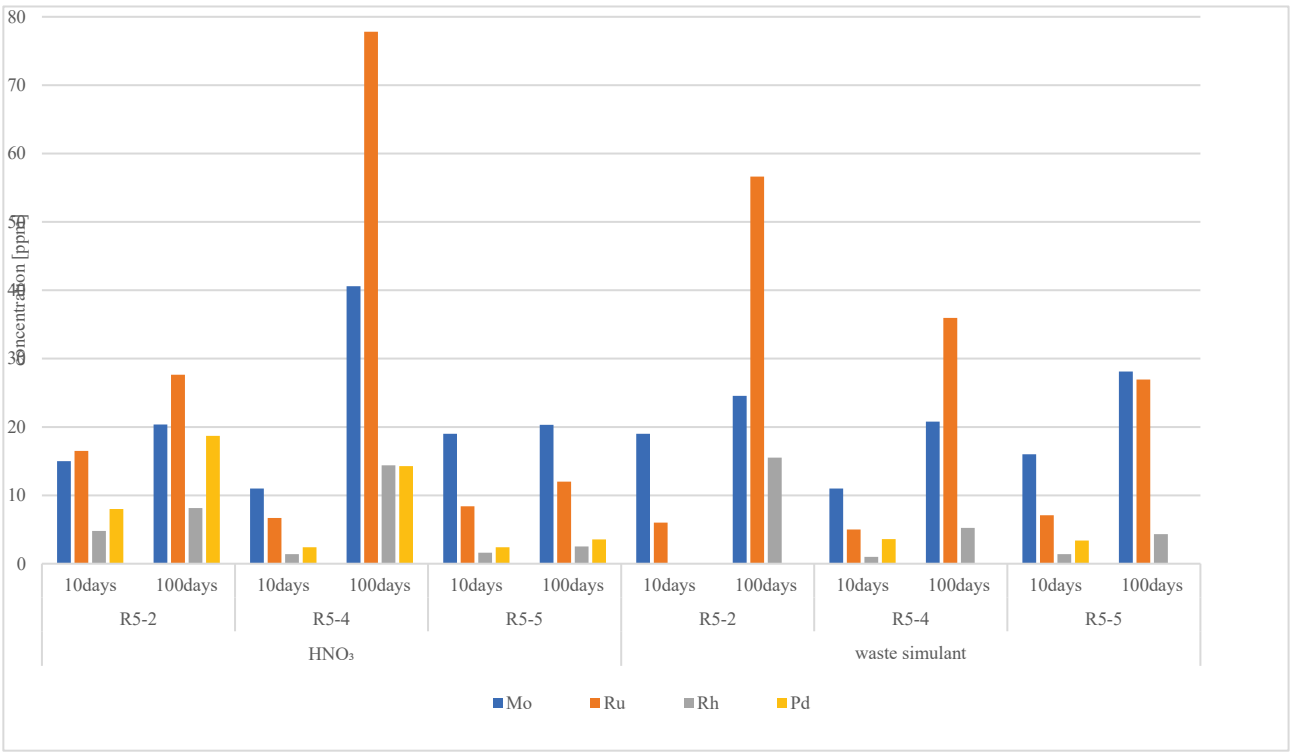

Fig. 2 Concentration of metal elements in dissolved solutions

Table 2 Alloy powder for the dissolution test; concentration and dissolution depth estimation results

ID	Alloy composition (Analytical value)				Solvent	Number of soaking days [days]	Concentration [ppm]				Estimated depth [nm]			
	Mo	Ru	Rh	Pd			Mo	Ru	Rh	Pd	Mo	Ru	Rh	Pd
R5-2	15.2	56.3	19.2	9.4	HNO_3	10	15	16.5	4.8	8	27.6	8.16	6.96	23.8
						100	20.4	27.6	8.1	18.7	37.6	13.7	11.8	55.9
					Liquid waste simulant	10	19	6			35.0	2.97		
						100	24.5	56.6	15.5		45.3	28.1	22.6	
R5-4	21.5	57.6	13.8	7.2	HNO_3	10	11	6.7	1.4	2.4	14.3	3.24	2.82	9.29
						100	40.6	77.8	14.4	14.3	53.1	37.8	29.2	55.8
					Liquid waste simulant	10	11	5	1	3.6	14.3	2.41	2.02	13.9
						100	20.8	36.0	5.2		27.0	17.4	10.6	
R5-5	30.1	51.1	12.1	6.7	HNO_3	10	19	8.4	1.6	2.4	17.6	4.57	3.68	9.97
						100	20.3	12	2.5	3.5	18.8	6.53	5.75	14.6
					Liquid waste simulant	10	16	7.1	1.4	3.4	14.8	3.86	3.22	14.1
						100	28.1	26.9	4.3		26.1	14.7	9.97	

by the transmission method for comparison substances and the fluorescence method for the residue.

2. Dissolution Test of Alloy Plate Sample

In particular, to clarify the dissolution behavior of the alloy surface, a novel simulated alloy R6-4 sample (Mo, 30; Ru, 50; Rh, 10; Pd, 10 wt%) was prepared using arc melting. R6-4 was produced for the same purpose and by the same manufacturing method as R5-5 that is explained in Sec. II.1. A low-speed cutter was used for plate processing, and the cut plate had the dimensions 2 mm × 2 mm × 1 mm. A magnetic stirring bar and one sample of the simulated alloy processed into a plate were placed in a beaker. Thereafter, 50 ml of 2.0 M nitric acid or liquid waste simulant was added, and a plate dissolution test was conducted for 10 days while magnetically stirring. The test was run at room temperature.

After the test was completed, only the alloy plate was recovered, and the top surface was analyzed using X-ray photoelectron spectroscopy (XPS) (SSX-100, Surface Science Instruments).

III. Results and Discussion

1. Dissolution Test Results of Alloy Powder Samples

(1) Concentration Analysis

Concentration analysis was performed on the dissolved solution using ICP-MS and ICP-OES. The concentrations of metal elements in it are shown in **Fig. 2**. From the Fig. 2 we could not confirm that the composition of the alloy and the type of dissolved solution affected the change in the dissolution amount. On the other hand, we did confirm that the amount of dissolution tended to increase with the dissolution time.

Further, the melting depth t [m] from the surface was calculated using the measured metal element concentration. The calculation method is shown below. Assuming that the concentration of metal elements in the solution is m_1 [ppm], the amount of dissolved solution is S [L], and the weight of the metal elements in the alloy is M [mg], we express the solubility X as

$$X = \frac{m_1 S}{M}. \tag{1}$$

If we simply ignore the deterioration due to corrosion or the like and consider that the volume decreases in proportion to the dissolved weight, then the volume v [m³] after dissolution, the volume V [m³] before dissolution, the radius r [m] of the sphere after dissolution, and the radius R [m] of the sphere before dissolution are related as follows.

$$\frac{v}{V} = \frac{\frac{4}{3}\pi r^3}{\frac{4}{3}\pi R^3} = \frac{r^3}{R^3} = 1 - X \tag{2}$$

From this equation, the radius r of the sphere after dissolution is

$$r = \sqrt[3]{(1-X) \times R^3} \tag{3}$$

and the dissolved depth t is

$$t = R - \sqrt[3]{(1-X) \times R^3} \tag{4}$$

from $t = R\text{-}r$.

Although the sample particle size varied from the results of the SEM image, the average particle size was around 10 μm, and the estimated dissolution depths assuming a particle size of 10 μm are shown in **Table 2**. From these dissolution depths, we confirmed that the macroscopic order of solubility was Mo>Pd>Ru>Rh. But, since the amount of Pd contained in the sample was small and measuring it was often impossible at the time of concentration analysis, we thought that it was better to keep it as a reference. In addition, since the solubility at 100 days was higher for all elements than at 10 days, the dissolution proceeded with the passage of time here as well.

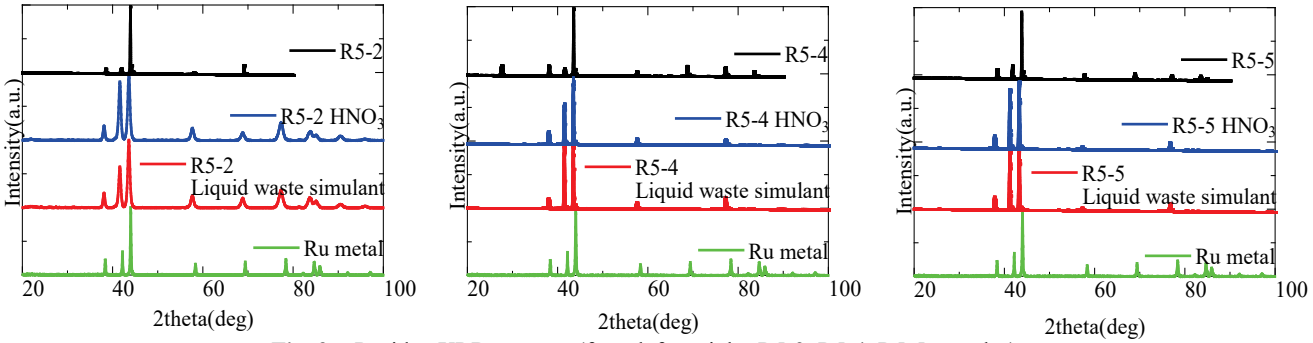

Fig. 3 Residue XRD patterns (from left to right: R5-2, R5-4, R5-5 samples)

(2) Crystal Structure Analysis

The XRD pattern of the dissolved residue is shown in **Fig. 3**. The crystal structure of the residue showed little change before and after dissolution. In addition, we confirmed that the peak position after dissolution was slightly smaller than before dissolution. The descending order of the peak shift, R5-5 > R5-2 > R5-4, suggested a change in structure due to alloy composition. On the other hand, there was almost no difference depending on the presence or absence of liquid waste components.

(3) Local Structural Analysis

Using XAFS, we performed local structural analysis of the residue neighborhoods known Mo and Ru regions. Due to the accessible energy of the device, Rh and Pd analyses were not performed. As a result, no significant change in the local structure after immersion was confirmed during 10 days of immersion, regardless of the alloy composition or the type of dissolved solution.

On the other hand, the results in the known Mo neighborhood during 100 days of immersion are shown in **Fig. 4** and **Fig. 5**. Further, the peak position of the Mo metal standard sample is shown by a dashed line in the figures. From Fig. 4, in the case of the dissolved solution being nitric acid, the peak in the first neighborhood of Mo in the Mo-rich R5-4 and R5-5 samples was smaller, and in the case of the dissolved solution in the liquid waste simulant from Fig. 5, both samples exhibited the characteristics of the first neighborhood peak of Mo.

Besides, in the neighborhood of Ru, there was not much change in the local structure after immersion (**Fig. 6** and **Fig. 7**).

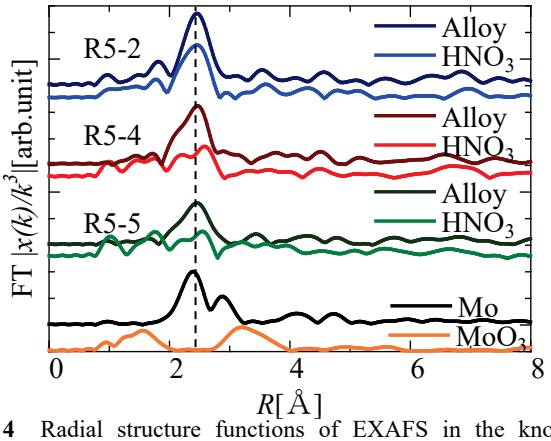

Fig. 4 Radial structure functions of EXAFS in the known neighborhood of Mo in residue after 100 days of dissolution with HNO_3.

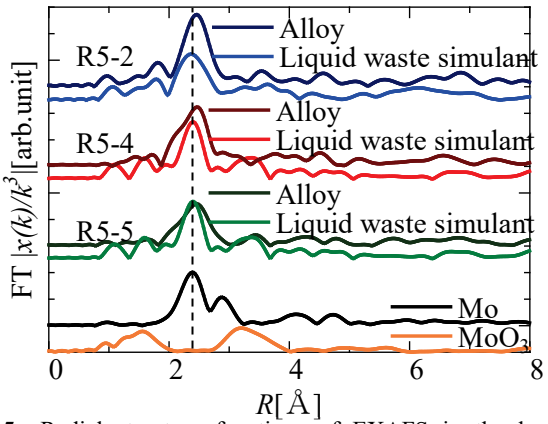

Fig. 5 Radial structure functions of EXAFS in the known neighborhood of Mo in residue after 100 days of dissolution with liquid waste simulant.

In general, the peaks in the radial structure functions of EXAFS depend on the coordination number, and distance between the target atom and ligand, so if a specific peak cannot be confirmed in the sample before and after dissolution, it is considered that the structure has changed due to dissolution. Therefore, from the above results, we found that the local structure of Mo changed with long-term dissolution, and that there was a dependence on the alloy composition. In addition, we considered that structural changes associated with dissolution were suppressed under the condition of coexisting liquid waste simulant.

Furthermore, even though dissolution occurred for all elements in Sec. III.1.(1), no change in the local structure in the neighborhood of Ru could be confirmed. This might be due to the fact that the solubility of Ru is lower than that of Mo, so there is no change inside, and the analysis depth of XAFS (several tens of micrometers[9]) does not fully grasp the dissolution behavior of the alloy only on the nanometer order surface.

2. Dissolution Test Results of Alloy Plate Sample

(1) Surface Analysis

Therefore, an R6-4 alloy sample was analyzed using XPS under five different conditions: before dissolution; after immersion in nitric acid or liquid waste simulant for 10 days and being etched only on the alloy surface (0 nm); and after immersion in nitric acid or liquid waste simulant and being etched to an arbitrary depth (2 to 10 nm).

The photoelectron spectra of the alloy plate samples are shown in **Fig. 8**. In addition, the literature data[10] of the peaks

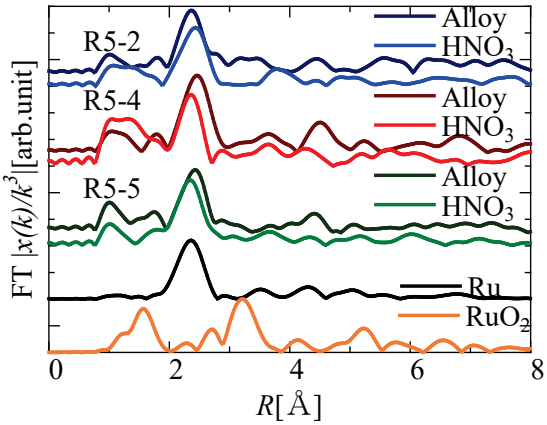

Fig. 6 Radial structure functions of EXAFS in the known neighborhood of Ru in residue after 100 days of dissolution with HNO_3.

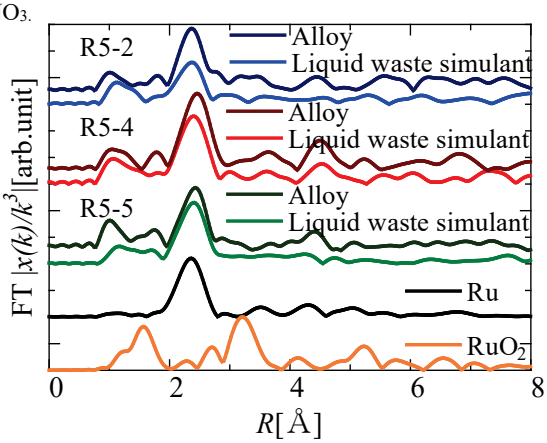

Fig. 7 Radial structure functions of EXAFS in the known neighborhood of Ru in residue after 100 days of dissolution with liquid waste simulant.

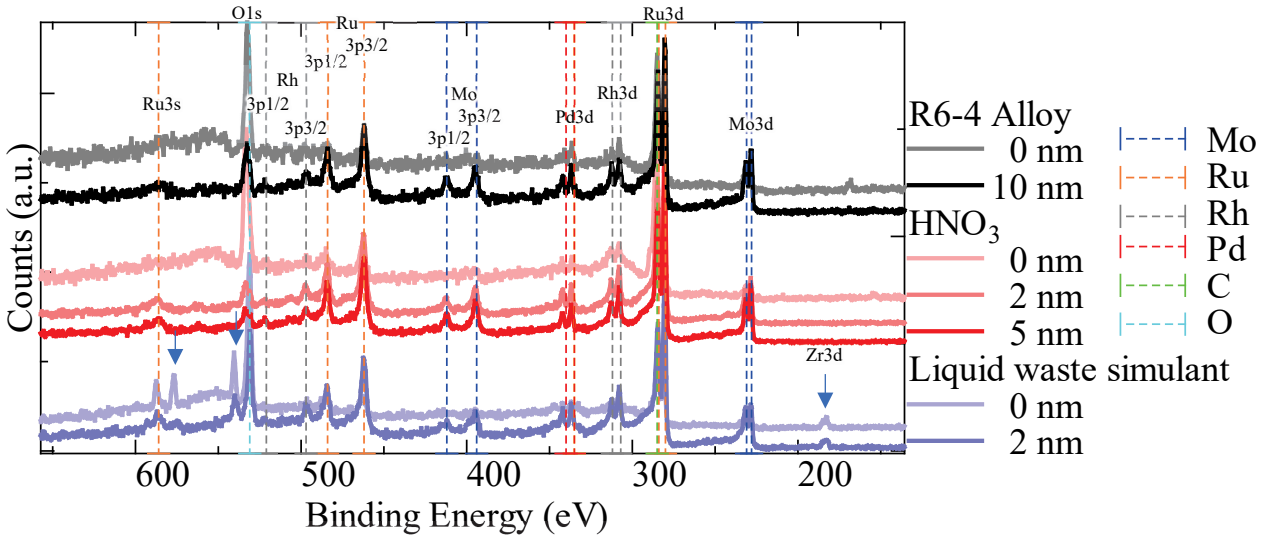

Fig. 8 Photoelectron spectra of alloy plate sample R6-4 for five sets of conditions (wide scan)

obtained for various metallic elements (Mo, blue; Ru, orange; Rh, gray; Pd, yellow) and C (yellow green) and O (light blue) are shown by dashed lines. From Fig. 8, peaks other than alloying elements and C and O were not confirmed before dissolution and after nitric acid dissolution, but after immersion in the liquid waste simulant, new peaks from other elements appeared at the positions indicated by the arrows. For example, we attributed peaks around 180 eV to the Zr 3d peak position when compared with the liquid waste simulant components,[10] suggesting that the liquid waste simulant components had penetrated to a depth of 2 nm.

Next, the results of the measurement focusing on the vicinity of the Mo 3d orbital are shown in **Fig. 9**. From this figure, the depth of 2 nm or more after nitric acid dissolution had a quite similar peak shape to the alloy before dissolution, and we considered that basically the sample existed in the alloy state. However, the peak position shifted slightly to the higher energy, suggesting a change in the bonding state or composition. On the other hand, the size and shape of the peak of the 3d5/2 orbital varied from 0 nm after nitric acid dissolution and varied 0 nm or more after liquid waste simulant dissolution compared to before dissolution, and a small shoulder appeared around 235 eV, so we considered they were not peaks of the alloy.

In addition, it was difficult to conclude that the change was due to dissolution because the effect of surface contamination appeared only on the surface (0 nm). Since no different peaks were observed at the 2 nm depth after nitrate dissolution, we thought that it was not necessary to take into account the effect of surface contamination at depths less than 2 nm. Therefore, we focused mainly on the results at depths of 2 nm and deeper.

Next, the results of the measurement focusing on the vicinity of the Ru 3d orbital are shown in **Fig. 10**, the results of the measurement focusing on the vicinity of the Rh3d orbital are shown in **Fig. 11**, and the results of the measurement focusing on the vicinity of the Pd 3d orbital are shown in **Fig. 12**. In all results, the peak shape at depths of 2 nm or more was similar to that of the alloy, and a slight peak shift was confirmed. Peak shifts are more pronounced for HNO_3 coexistence.

In addition, **Fig. 13** shows results focusing on the vicinity of the O 1s orbital. From this figure, a slight peak in the O 1s

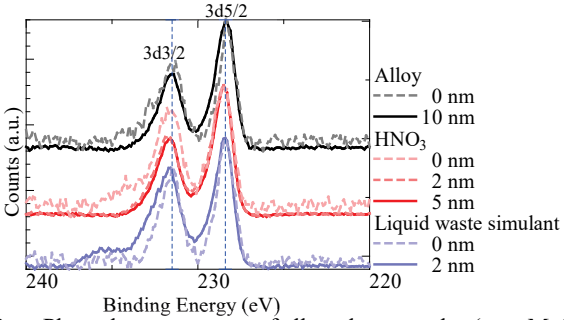

Fig. 9 Photoelectron spectra of alloy plate samples (near Mo3d).

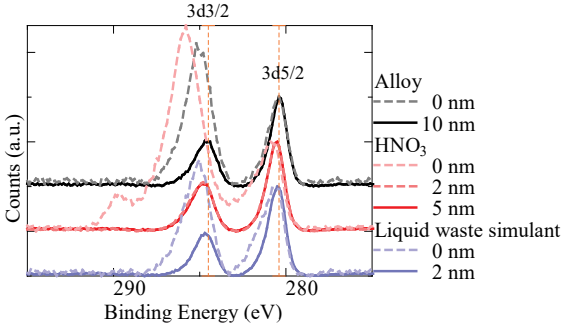

Fig. 10 Photoelectron spectra of alloy plate samples (near Ru3d).

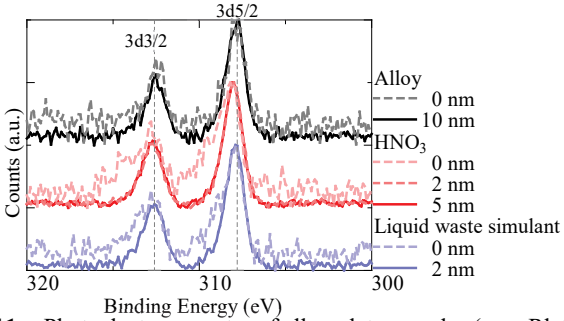

Fig. 11 Photoelectron spectra of alloy plate samples (near Rh 3d).

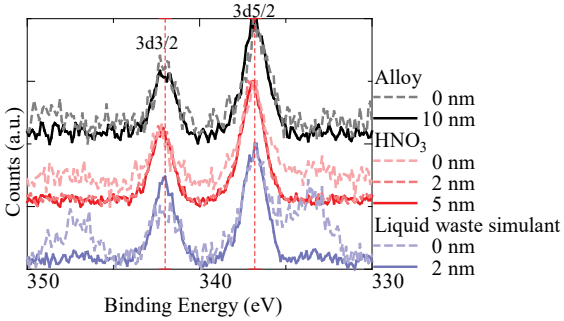

Fig. 12 Photoelectron spectra of alloy plate samples (near Pd3d).

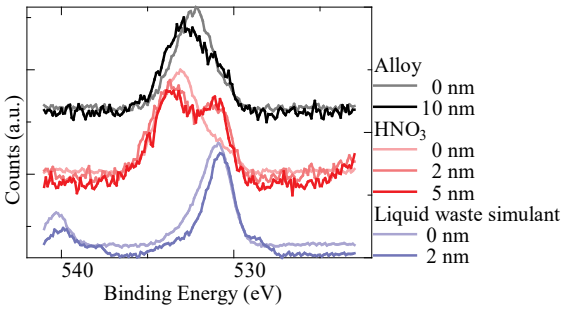

Fig. 13 Photoelectron spectra of alloy plate samples (near O1s).

orbital was confirmed around 533 eV at 0 nm of the alloy sample that had not been immersed, which we thought was reasonable because it did not originally contain oxygen. We speculated that this was due to the effects of surface contamination. On the other hand, at 0 nm after immersion in nitric acid and liquid waste simulant, peaks appeared at different positions around 530 to 535 eV, which was considered to be the effect of each immersion liquid rather than surface contamination, and we presumed that the chemical form of oxygen was different due to alloy corrosion.

The spectra seen in XPS were composite peaks produced by the bonding energy peaks of elements in different chemical states. Therefore, if the distances between overlapping peaks were close to each other, it would look like one large peak, and a peak shift would occur when the type and intensity of the overlapping peaks change. Therefore, we presumed that the metal elements in the alloy became a compound when they came into contact with nitric acid and dissolved.

In addition, in the case of Ru, Rh, and Pd in the presence of liquid waste simulant, the peak shift was small, that is, the extent of formation of compounds was small, which was inferred to be due to suppressed dissolution, and that was consistent with the view presented in Sec. III.1.(3). Since the peak shape of Mo changed in the presence of liquid waste simulant, and the presence of Zr and O was also confirmed, we speculated that the presence of liquid waste components might have caused the formation of Mo compounds on the surface, which became a protective layer and suppressed dissolution. In addition, since we could not confirm this using comparable results for possible compounds other than pure oxides, we could not identify the bonding state.

IV. Conclusion

In this study, we conducted two kinds of dissolution tests to elucidate the dissolution behavior of platinum group alloys when coexisting with nitric acid or liquid waste simulant.

The solubility of the alloy elements was Mo>Ru>Rh regardless of composition, and the dissolution progressed with time. In addition, findings suggested that one or more compounds were formed on dissolution, and that Mo which has a high solubility rate seemed to be dissolved more internally. In particular, alloys with a high Mo ratio tended to have a large impact on the interior, so there would be a risk of composition fluctuations.

On the other hand, dissolution was suppressed for the coexisting liquid waste simulant, and we speculated that the liquid waste simulant components promoted the formation of Mo compounds and formed a protective layer on the surface.

From the results of this study, we confirmed that by conducting a micro-level evaluation using XPS, differences not seen in the macro-level evaluation with XAFS were observed, demonstrating the usefulness of XPS. On the other hand, the surface was significantly affected by surface contamination, such as from nitric acid, making evaluation difficult. Therefore, it is necessary to conduct surface evaluations much deeper into the material.

Acknowledgment

This presentation is part of the results of the project "Basic Research Project (JPJ010599) on vitrification technology for reducing the volume of radioactive waste in FY Reiwa 5 and 6" supported by the Agency for Natural Resources and Energy of the Ministry of Economy, Trade and Industry (METI).

Part of this research was supported by the Center for Interdisciplinary Research in Nano Science and Technology, Tokyo City University.

The XAFS measurements were carried out using the BL27B of the KEK Photon Factory (Proposal Nos. 2020G606 and 2022G618), and using the BL11N2 of the Aichi Synchrotron Radiation Center, Aichi Science & Technology Foundation, Aichi, Japan (Proposal Nos. 202204045, 202204067, and 202205056).

References

1) I. Yamagishi, M. Odakura, Y. Ichige, M. Kuroha, M. Takano, M. Akabori, M. Yoshioka, "Chemical composition of insoluble residue generated at the Rokkasho Reprocessing Plant," *Proceedings of 21st International Conference & Exhibition; Nuclear Fuel Cycle for a Low-Carbon Future*, 1113-1119 (2015).
2) H. Aihara, Y. Arai, A. Shibata, K. Nomura, M. Takeuchi, "Characterization of the Insoluble Sludge from the Dissolution of Irradiated Fast Breeder Reactor Fuel," *Procedia Chemistry*, **21**, 279-284 (2016).
3) T. Akai, J. Nishii, M. Yamashita, H. Yamanaka, "Chemical behavior of platinum-group metals in oxide glasses," *Journal of Non-Crystalline Solids*, **222**, 304-309 (1997).
4) B. Luckscheiter, M. Nesovic, "Development of glasses for the vitrification of high level liquid waste (HLLW) in a joule heated ceramic melter," *Waste Management*, **16**[7], 571-578 (1996).
5) A. Sakai, S. Ishida, "Reflective reviews on Japanese high-level waste (HLW) vitrification - Exploring the obstacles encountered in active tests at Rokkasho," *Annals of Nuclear Energy*, **196**, (2024).
6) K. Yamazaki, N. Tarumi, I. Sato, H. Tada, H. Matsuura, "Oxidation Behavior of Platinum Group Alloys in Molten Glass." *Electrochemistry*, **92**[4], (2024).
7) T. Matsui, "Research on nitric acid dissolution of fission precious metal alloys." *PNC TJ1603 92-003*, (1992). [in Japanese]
8) T. Adachi, M. Ohnuki, N. Yoshida, T. Sonobe, W. Kawamura, H. Takeishi, K. Gunji, T. Kimura, T. Suzuki, Y. Nakahara, T. Muromura, Y. Kobayashi, H. Okashita, T. Yamamoto, "Dissolution study of spent PWR fuel: Dissolution behavior and chemical properties of insoluble residues," *Journal of Nuclear Materials*, **174**[1], 60-71 (1990).
9) K. Okumura, K. Sugino, K. Kojima, T. Jin, T. Okamoto, J. Katakura, "A Set of ORIGEN2 Cross Section Libraries Based on JENDL-4.0: ORLIBJ40," *JAEA-Data/Code 2012-032*, (2013)
10) T. Nomoto, "About Controlling Analysis Depth in XAFS," *Aichi Center for Industrial Science and Technology News*, **2015**[12], (2015). [in Japanese]
11) "NIST X-ray Photoelectron Spectroscopy Database," NIST Standard Reference Database Number 20, National Institute of Standards and Technology, Gaithersburg MD, 20899 (2000), DOI: https://dx.doi.org/10.18434/T4T88K, (retrieved [28/10/2024]).